Research Article

Mathematical Methods in the Applied Sciences

Received XXXX

(www.interscience.wiley.com) DOI: 10.1002/sim.0000
MOS subject classification: XXX; XXX

Three-point bending tests. Part II: An improved formula for the modulus of rupture and numerical simulations

F. Guitián[b] and P. Quintela[a]* and M. T. Sánchez[a] and V. Valcárcel[b]

The goal of this paper is to analyze analytical and numerically, from several perspectives, the modulus of rupture (MOR) for brittle materials, studying the bending test of three points which is normally used in laboratory to calculate it. In particular, we will give four different approaches to the MOR: through the classical theory of beams; by means of the one and three-dimensional numerical simulations; and by using an improved expression to the MOR obtained through its asymptotic analysis. Finally, we will present these methodologies for cylindrical and rectangular beams made of porcelain.

Keywords: Modulus of rupture; contact conditions; numerical simulations.

1. Introduction

The relative simplicity of the bending tests has permitted its popularization for measuring the mechanical properties of brittle materials (see [1]). For example, the three-point bending test is hugely used to calculate the modulus of rupture (MOR): the maximum surface stress of the bent beam at the instant of failure (see Fig. 1). In the engineering literature, the MOR is calculated by an explicit formula which involves the value of the load at failure, H, the distance, $2l$, between the two supports, and the second moment of inertia, I_1, of the transversal section of the beam (see [2]).

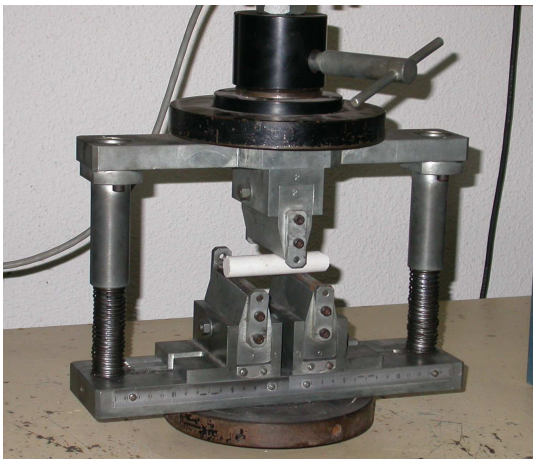

Figure 1. Three-point bending test.

[a] *Department of Applied Mathematics. Universidade de Santiago de Compostela, 15782 Santiago de Compostela, Spain.*
[b] *Institute of Ceramics. Universidade de Santiago de Compostela, 15782 Santiago de Compostela, Spain.*
* *Correspondence to: Tel.: +34-981-563-100; fax: +34-981-597-054, peregrina.quintela@usc.es*

Prepared using mmaauth.cls [Version: 2009/09/02 v2.00]

Nevertheless, discrepancies by no means negligible for MOR values have been noticed in experimental measurements depending on the specimen size, the ratio between the area of its section and the overall length or the relation between the distance of the two lower cylinders and the overall length of the beam. The fact that samples of same material can lead to different values for the MOR is something quite common but so far there are not many studies about this behaviour. In order to increase the knowledge about the MOR for brittle materials we have carried out a complete mathematical analysis of the three-point bending test (see [3]): a result of existence and uniqueness of a solution for the associated mathematical model has been proved, and, in order to justify the classic formula to the MOR, the corresponding one-dimensional problems for bending and for traction have been obtained by means of the asymptotic expansion method.

In this work we are interested in finding an effective method to compute the MOR from brittle materials. To do this, we will use all the theoretical background collected in [3] to compute various approximations of the MOR. The procedure is the following: Once we have carried out several laboratory tests with ceramic beams, we will determine the maximum force that beams can support until breaking –the force of rupture. By using the classic expression for the MOR, we will calculate the first value for it –the theoretical MOR. Then, after making numerical simulations of the one and three-dimensional models, considering the rupture load, we will compute two new approximations for the MOR –the 1d and 3d numerical MOR. Finally, we will obtain a fourth approach for the MOR by using a new expression obtained from the asymptotic analysis of our problem. All these methodologies are applied for cylindrical and rectangular beams made of porcelain, which is a brittle material used very frequently in engineering.

As we will see in the conclusions, the new theoretical formula obtained in this paper will lead us to a better approximation of the MOR for brittle materials. This expression takes into account not only the rupture load and the total length of the beam but also the distance between the two lower cylinders, the effect of the gravity and the distance between the ends of the beam and the lower cylinders.

The outline of the paper is as follows. In Section 2, we will describe the three-point bending test and we will introduce the classic formula for the MOR of brittle materials. Section 3 is devoted to recall the mathematical model associated with this experiment: an elastic problem with a frictionless unilateral contact condition. We will summarize the assumptions of compatibility on the forces needed to obtain the existence of a unique solution of the associated variational problem. Several examples for laboratory tests for cylindrical and rectangular beams are detailed in Section 4. We will show that the previous compatibility assumptions are satisfied for these real experiments. In Section 5, we will obtain, from the differential formulation of the bending and axial displacements obtained by using the asymptotic analysis, analytical solutions for some tests. Moreover, we will introduce the new theoretical expression for the MOR. In Section 6, we will gather all the approaches for the MOR of the porcelain by using the methodology described above. We will apply this procedure for both cylindrical and rectangular beams. Finally, in Appendix A we will offer a brief description of the classic expression for the MOR used in mechanics of materials given that this information is not usually included in the mathematical bibliography.

2. The theoretical MOR

In three-point bending tests a sample of a brittle material is placed between three cylinders, without additional support, while with the upper cylinder applies an increasing gradually force until the beam breaks (see Fig. 1). Although the applied force, H, is very close to a "Dirac's delta" distribution, to simplify the calculations we assume that it is applied on a small part Γ_{N_1} of the lateral boundary and is of constant density. Then, the rupture load is $\mathbf{H} = -H\mathbf{e}_2 = -h\text{Area}(\Gamma_{N_1})\mathbf{e}_2$, where h and H are positive constants. The resultant, H, is measured in laboratory.

In the classical theory of beams, the MOR is given by an explicit expression which involves the value of the load of failure, H, the distance, $2l$, between the two lower cylinders, and the second moment of inertia, I_1, of the transversal section of the beam (see [2]).

In particular, the theoretical MOR of a cylindrical beam with radius R subjected to a failure load with modulus H is

$$\sigma_{ft} = \frac{2Hl}{\pi R^3}; \tag{1}$$

analogously, if the beam is rectangular with width $2a$ and height $2b$, the theoretical MOR is

$$\sigma_{ft} = \frac{3Hl}{8ab^2}. \tag{2}$$

A brief explanation on the classic expression for the MOR will be presented later in Appendix A.

3. Mathematical model

Let ω be a bounded, open, connected domain in $\mathbb{R}^2$; we consider a beam which occupies at rest the domain $\overline{\Omega} = \overline{\omega} \times [-L, L], L > 0$, and we refer the motion of the beam to a fixed Cartesian system $Ox_1x_2x_3$ whose origin is situated at the center of gravity of

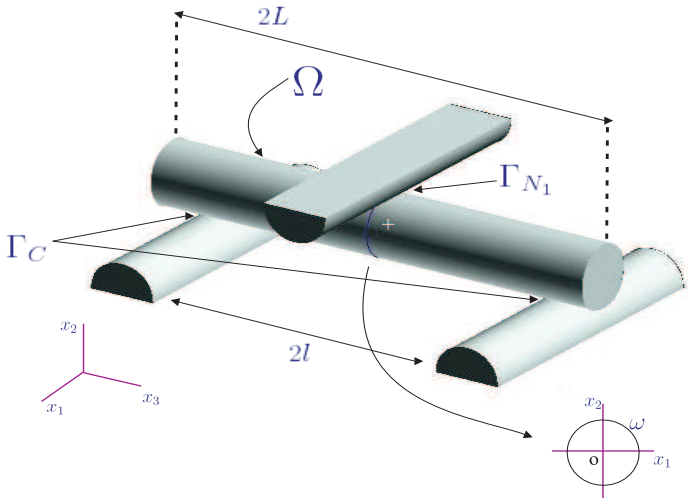

Figure 2. Sketch of three-point bending test.

the beam (see Fig. 2). Hereafter, Latin subscripts are understood to range over the integers $\{1, 2, 3\}$ and Greek subscripts over the integers $\{1, 2\}$. Moreover, summation over repeated subscripts is implied.

The physical problem consists of determining the displacement vector field, $\mathbf{u}$, and the stress tensor field, $\boldsymbol{\sigma}$, that the beam $\bar{\Omega}$ suffers when it is subjected to a three-point bending test.

Let Γ be the boundary of the beam which is the union of the lateral boundary Γ_l and the ends $\Gamma_\pm = \omega \times \{\pm L\}$, $\mathbf{n}$ being the outward unit normal vector to Γ. Γ_l is partitioned into three non-empty, open and disjointed parts Γ_C, Γ_{N_1} and Γ_{N_2}, where Γ_C is the region of the beam resting on the two lower cylinders for which we impose a Signorini frictionless contact condition (see [4]); Γ_{N_1} corresponds to the region of the boundary in which the upper cylinder exerts a compression force of known resultant, H, and Γ_{N_2} represents the remaining lateral boundary of the beam that is free of forces. The ends of the beam are also assumed to be free of forces.

The most used materials in three-point bending tests are brittle materials that break suddenly, being its response, until the moment of failure, almost elastic and linear. Then, we assume that the infinitesimal strain field, $\boldsymbol{\varepsilon}(\mathbf{u})$, is related to the stress tensor, $\boldsymbol{\sigma}$, through Hooke's law and that the material is homogeneous and isotropic.

Under the assumption of small displacements, the behavior of the beam is governed by the usual equilibrium equations:

Problem *(P)*:

Find the displacement vector field, $\mathbf{u}(\mathbf{x})$, and the stress tensor field, $\boldsymbol{\sigma}(\mathbf{x})$, at each point $\mathbf{x} \in \Omega$, satisfying:

$$-\mathrm{div}(\boldsymbol{\sigma}) = \mathbf{f} \text{ in } \Omega, \tag{3}$$

$$\boldsymbol{\sigma}\mathbf{n} = \mathbf{h} \text{ on } \Gamma_{N_1}, \tag{4}$$

$$\boldsymbol{\sigma}\mathbf{n} = \mathbf{0} \text{ on } \Gamma_{N_2} \cup \Gamma_\pm, \tag{5}$$

$$\boldsymbol{\sigma}_\tau = \mathbf{0},\ \sigma_n \leq 0,\ u_n \leq 0,\ \sigma_n u_n = 0 \text{ on } \Gamma_C, \tag{6}$$

$$\boldsymbol{\sigma} = \Lambda\boldsymbol{\varepsilon}(\mathbf{u}) = \lambda \mathrm{tr}(\boldsymbol{\varepsilon}(\mathbf{u}))\mathbf{I} + 2\mu\boldsymbol{\varepsilon}(\mathbf{u}) \text{ in } \Omega, \tag{7}$$

where u_n is the normal component of $\mathbf{u}$ and σ_n and $\boldsymbol{\sigma}_\tau$ are the normal and tangential components of $\boldsymbol{\sigma}\mathbf{n}$, respectively. In (7), λ and μ are the Lamé parameters of the material, related with Young's modulus, E, and Poisson's ratio, ν, by the usual expressions.

3.1. Mathematical analysis of Problem (P)

In [3], we have carried out the mathematical analysis of Problem (P), associated with the three-point bending test. Next, we will summarize the most important results obtained therein.

We consider the space of displacement vector fields $\mathbf{H}^1(\Omega) = [H^1(\Omega)]^3$ and the convex subset of kinematically admissible displacements

$$\mathbf{K}(\Omega) = \{\mathbf{v} \in \mathbf{H}^1(\Omega);\ v_n \leq 0 \text{ on } \Gamma_C\}.$$

The corresponding space of stress fields is defined by

$$\mathbf{X}(\Omega) = \{\boldsymbol{\tau} = (\tau_{ij});\ \boldsymbol{\tau} \in [L^2(\Omega)]^9,\ \tau_{ij} = \tau_{ji}\}.$$

From now on we consider the following hypotheses.

(H1) The volume forces satisfy $\mathbf{f} \in \mathbf{L}^2(\Omega)$ and the surface forces $\mathbf{h} \in \mathbf{L}^2(\Gamma_{N_1})$.

(H2) The material is homogeneous and isotropic; so, the elasticity tensor $\mathbf{\Lambda}$ defined in (7) is such that $\lambda, \mu \in \mathbb{R}$, $\lambda, \mu > 0$.
(H3) The applied forces verify the compatibility condition

$$\int_\Omega \mathbf{f} \cdot \mathbf{w} d\mathbf{x} + \int_{\Gamma_{N_1}} \mathbf{h} \cdot \mathbf{w} d\Gamma \leq 0,$$

for all $\mathbf{w} \in \mathbf{K}(\Omega) \cap \mathbf{R}(\Omega)$, where

$$\mathbf{R}(\Omega) = \{\mathbf{w} \in \mathbf{H}^1(\Omega) : \boldsymbol{\varepsilon}(\mathbf{w}) = \mathbf{0} \text{ in } [L^2(\Omega)]^9\}, \tag{8}$$

is the set of rigid displacements. Moreover,

$$\int_\Omega \mathbf{f} \cdot \mathbf{w} d\mathbf{x} + \int_{\Gamma_{N_1}} \mathbf{h} \cdot \mathbf{w} d\Gamma = 0,$$

if and only if $\mathbf{w} \in \mathbf{R}_n(\Omega)$, where

$$\mathbf{R}_n(\Omega) = \{\mathbf{w} \in \mathbf{R}(\Omega); w_n = 0 \ a.e. \text{ on } \Gamma_C\}.$$

(H4) The set $(\mathbf{K}(\Omega) \cap \mathbf{R}(\Omega)) \setminus \mathbf{R}_n(\Omega)$ is non-empty.
(H5)
- Domain ω is symmetrical with respect to the lines $x_1 = 0$ and $x_2 = 0$.
- Boundaries Γ_{N_1} and Γ_C are symmetrical with respect to the planes $x_1 = 0$ and $x_3 = 0$. Furthermore,

$$\Gamma_{N_1} = \{\mathbf{x} \in \Gamma_l; |x_3| < \delta, (x_1, x_2) \in \gamma_{N_1}(x_3)\},$$
$$\Gamma_C = \{\mathbf{x} \in \Gamma_l; 0 < |x_3| - l < \hat{\delta}, (x_1, x_2) \in \gamma_C(x_3)\},$$

  with $\gamma_{N_1}(x_3), \gamma_C(x_3) \subset \gamma$, and δ, $\hat{\delta}$ being small parameters, verifying $\delta < l - \hat{\delta}$.
- The second component of the outward normal vector to Γ is not null on Γ_C and with constant sign. Moreover, it is even with respect to x_1.

(H6) Volume and surface forces verify that

- f_1 and h_1 are odd with respect to x_1 and even with respect to x_3,
- f_2 and h_2 are even with respect to x_1 and x_3,
- f_3 and h_3 are even with respect to x_1 and odd with respect to x_3.

The weak formulation corresponding to Problem (P) is the following:
Problem *(VP)*:

$$\left\{ \begin{array}{l} \text{Find } \mathbf{u} \in \mathbf{K}(\Omega) \text{ such that} \\ \displaystyle\int_\Omega \Lambda\boldsymbol{\varepsilon}(\mathbf{u}) : \boldsymbol{\varepsilon}(\mathbf{v} - \mathbf{u}) d\mathbf{x} \quad \geq \quad \int_\Omega \mathbf{f} \cdot (\mathbf{v} - \mathbf{u}) d\mathbf{x} + \int_{\Gamma_{N_1}} \mathbf{h} \cdot (\mathbf{v} - \mathbf{u}) d\Gamma, \\ \qquad\qquad\qquad\qquad \forall \mathbf{v} \in \mathbf{K}(\Omega). \end{array} \right. \tag{9}$$

By using a well-known result of Fichera (see [5]), we have established the existence of a unique solution of Problem (PV) (see [3]):

Theorem 1. *i) Under assumptions* **(H1)-(H4)**, *there exists a solution of Problem* (VP).
ii) Under assumptions **(H1)-(H6)**, *there exists a unique solution* $\mathbf{u} \in \mathbf{H}_s(\Omega) \cap \mathbf{K}(\Omega)$ *of Problem* (VP), $\mathbf{H}_s(\Omega)$ *being the set:*

$$\mathbf{H}_s(\Omega) = \left\{ \mathbf{v} \in \mathbf{H}^1(\Omega); \begin{array}{l} v_1 \text{ is odd in } x_1 \text{ and even in } x_3 \\ v_2 \text{ is even in } x_1 \text{ and } x_3 \\ v_3 \text{ is even in } x_1 \text{ and is odd in } x_3 \end{array} \right\}.$$

4. Verifying hypotheses for two laboratory experiences

In this section, we describe in detail the two real cases of bending tests carried out in laboratory. For both numerical results will be presented in later sections.

4.1. Description of data of the experiments

In the following, we present a description of the geometry of the samples, of the different regions considered at the boundary and of the applied forces. In three-point bending tests, the boundary Γ_{N_1} corresponds to the region of contact between the beam and the upper cylinder, which is assumed to be known in advance. In this region, the force is applied vertically to the beam and its resultant, $\mathbf{H} = -H\mathbf{e}_2$, $H > 0$, is measured in laboratory. In practice (see Fig. 1), this force is very close to a "Dirac's delta" distribution, which can be approached in numerical simulations as top hat functions defined on small areas and with the same resultant. In effect, according to Saint Venant's principle (see [6]), if a body is submitted to a system of forces acting over a

bounded region of its surface, stresses and strains induced away from this region do not depend on the particular form of the applied force, but rather on its resultant. Taking into account that our objective is to compute the MOR, which depends only on the stresses induced in the region opposite to Γ_{N_1}, in order to simplify the computations, we assume that the applied force is a top hat function with constant density, h,

$$\mathbf{h} = -h\mathbf{e}_2,\ h = \frac{H}{\text{area}(\Gamma_{N_1})}.$$

The contact boundary, Γ_C, corresponds to the region where the beam may come into contact with the two lower cylinders; while Γ_C is fixed in advance, the actual contact area is, of course, a priori unknown.

The only volume force acting on the beam is due to the action of the gravity and its expression is

$$\mathbf{f} = -\rho g\mathbf{e}_2,$$

where ρ is the density of the material and g is the gravitational acceleration. In both experiments we consider, as brittle material, the porcelain.

We detail below the two considered experiments.

Experiment I: Cylindrical beams.

In this first case, we are going to use a system of cylindrical coordinates $\{r, \theta, z\}$. We consider a beam of length $2L$ whose section is a circle of radius R and we assume that there is a distance $2l$ between the two lower cylinders. The geometry of the beam can be expressed by

$$\Omega = \{(r, \theta, z); r \in [0, R), \theta \in [0, 2\pi), z \in (-L, L)\}. \tag{10}$$

The expression for the boundary Γ_{N_1} is

$$\Gamma_{N_1} = \{(R, \theta, z); \theta \in \left(\frac{\pi}{2} - \delta, \frac{\pi}{2} + \delta\right), z \in (-\delta, \delta)\}, \tag{11}$$

where δ is a positive parameter and small enough to assure that the resultant force on Γ_{N_1} is $\mathbf{H}$; therefore,

$$\delta = \left(\frac{H}{4hR}\right)^{1/2}.$$

The contact boundary, Γ_C, is given by the expression

$$\Gamma_C = \{(R, \theta, z); \theta \in \left(\frac{3\pi}{2} - \frac{\hat{\delta}}{2}, \frac{3\pi}{2} + \frac{\hat{\delta}}{2}\right), z \in (-l - \hat{\delta}, -l) \cup (l, l + \hat{\delta})\}, \tag{12}$$

where $\hat{\delta}$ is the thickness of the contact zone between the beam and each lower cylinder; $\hat{\delta}$ is a positive parameter and small.

Experiment II: Rectangular beams.

In the second experiment, we use rectangular beams of length $2L$, width $2a$ and height $2b$, so their geometry is described as

$$\Omega = (-a, a) \times (-b, b) \times (-L, L).$$

The expression of the boundary Γ_{N_1} is

$$\Gamma_{N_1} = \{(x_1, b, x_3); x_1 \in (-a, a), x_3 \in (-\delta, \delta)\}, \tag{13}$$

where, again, 2δ is chosen such that the resultant force on Γ_{N_1} is $\mathbf{H}$:

$$\delta = \frac{H}{4ha}.$$

The contact boundary, Γ_C, is given by the expression

$$\Gamma_C = \{(x_1, -b, x_3); x_1 \in (-a, a), x_3 \in (-l - \hat{\delta}, -l) \cup (l, l + \hat{\delta})\}, \tag{14}$$

where, again, $\hat{\delta}$ is the thickness of the contact zone between the beam and each lower cylinder.

4.2. Behaviour of applied forces

As we have recalled in Section 3, there exists a unique solution of Problem (VP) if assumptions **(H1)**-**(H6)** are verified. In this section, we focus on prove that the assumption **(H3)** is satisfied for both experiments I and II. For this, first, we are going to characterize the expression of rigid displacements.

4.2.1. Characterization of rigid displacements The following lemma identifies the elements of $\mathbf{R}(\Omega)$ defined by (8).

Lemma 1. *The following conditions are equivalent:*

(i) $\mathbf{w} \in \mathbf{R}(\Omega)$,
(ii) $\mathbf{w}(\mathbf{x}) = \mathbf{c} + \mathbf{d} \times \mathbf{x}$, *a.e. in* Ω, *with* $\mathbf{c}, \mathbf{d} \in \mathbb{R}^3$,
(iii) $\mathbf{w}(r, \theta, z) = w_r \mathbf{e}_r + w_\theta \mathbf{e}_\theta + w_z \mathbf{e}_z$, *where*

$$\begin{aligned} w_r &= (A \sin\theta + B\cos\theta) + z(C \sin\theta + D\cos\theta), \\ w_\theta &= (A\cos\theta - B \sin\theta) + z(C\cos\theta - D \sin\theta) + Er, \\ w_z &= F - r(C \sin\theta + D\cos\theta), \end{aligned}$$

a.e. in Ω, *with* $A, B, C, D, E, F \in \mathbb{R}$,

where $\times$ *denotes the vectorial product,* $\mathbf{x}$ *is the position vector of the point* (x_1, x_2, x_3) *and* (r, θ, z) *are the cylindrical coordinates of* $\mathbf{x}$ *in* Ω.

Proof. Equivalence between *(i)* and *(ii)* can be seen in Theorem 3.2 of Chapter 6 in [7]. Implication *(iii)*$\rightarrow$ *(i)* is obvious if we take into account the expression of the infinitesimal strain field in cylindrical coordinates (see [8]).

We are going to prove the implication *(i)*$\rightarrow$ *(iii)*. We have that $\mathbf{w} \in \mathbf{R}(\Omega)$, so it means in cylindrical coordinates

$$0 = \varepsilon_{rr}(\mathbf{w}) = w_{r,r}, \tag{15}$$

$$0 = \varepsilon_{\theta\theta}(\mathbf{w}) = \frac{1}{r} w_{\theta,\theta} + \frac{w_r}{r}, \tag{16}$$

$$0 = \varepsilon_{zz}(\mathbf{w}) = w_{z,z}, \tag{17}$$

$$0 = 2\varepsilon_{r\theta}(\mathbf{w}) = w_{\theta,r} + \frac{1}{r} w_{r,\theta} - \frac{w_\theta}{r}, \tag{18}$$

$$0 = 2\varepsilon_{\theta z}(\mathbf{w}) = \frac{1}{r} w_{z,\theta} + w_{\theta,z}, \tag{19}$$

$$0 = 2\varepsilon_{rz}(\mathbf{w}) = w_{r,z} + w_{z,r}. \tag{20}$$

By using (15), (17) and (20) we have

$$w_r = f_1(\theta) + f_2(\theta) z, \tag{21}$$

$$w_z = \hat{f}_1(\theta) + \hat{f}_2(\theta) r, \tag{22}$$

with

$$f_2(\theta) = -\hat{f}_2(\theta). \tag{23}$$

Deriving with respect to z in (19) and by using (17) we have that $w_{\theta,zz} = 0$. Again, deriving with respect to r in (19) and by using (22), we obtain

$$w_{\theta,zr} = \frac{1}{r^2} \hat{f}_1'(\theta). \tag{24}$$

Deriving with respect to z in (18) and by using (21) and (24) we can write

$$w_{\theta,z} = \frac{1}{r} \hat{f}_1'(\theta) + f_2'(\theta), \tag{25}$$

and deriving now with respect to r

$$w_{\theta,zr} = -\frac{1}{r^2} \hat{f}_1'(\theta). \tag{26}$$

Expressions (24) and (26) lead to the condition

$$\hat{f}_1'(\theta) = 0 \quad \forall \theta \in [0, 2\pi) \Rightarrow \hat{f}_1(\theta) = \hat{f}_1 \in \mathbb{R} \quad \forall \theta \in [0, 2\pi). \tag{27}$$

Therefore, from (22), (23), (25) and (27) we have the expressions

$$w_\theta = f_2'(\theta) z + f_3(r, \theta), \tag{28}$$

$$w_z = \hat{f}_1 - f_2(\theta) r. \tag{29}$$

Substituting (21), (28) and (29) in (16) and (18), we obtain

$$0 = (f_2''(\theta) + f_2(\theta))z + f_1(\theta) + f_{3,\theta}, \tag{30}$$

$$0 = f_{3,r} - \frac{1}{r} f_3(r,\theta) + \frac{1}{r} f_1'(\theta). \tag{31}$$

Deriving with respect to r in (30) and with respect to θ in (31), we deduce

$$0 = f_{3,r\theta},$$

$$0 = -\frac{1}{r} f_{3,\theta} + \frac{1}{r} f_1''(\theta),$$

and then

$$f_{3,\theta} = f_1''(\theta).$$

Therefore, we have

$$f_3(r,\theta) = f_1'(\theta) + f_4(r). \tag{32}$$

In addition, substituting (32) in (31), we obtain that f_4 must verify the ordinary differential equation:

$$f_4'(r) = \frac{1}{r} f_4(r),$$

whose general solution is

$$f_4(r) = f_4 r, \quad f_4 \in \mathbb{R};$$

this leads to the following expression for f_3:

$$f_3(r,\theta) = f_1'(\theta) + f_4 r. \tag{33}$$

Finally, substituting the previous expression in (30), we have

$$0 = (f_2''(\theta) + f_2(\theta))z + (f_1''(\theta) + f_1(\theta)), \quad \forall (\theta, z) \in [0, 2\pi) \times (-L, L), \tag{34}$$

so we obtain the homogeneous ordinary differential equations for f_1 and f_2:

$$f_1''(\theta) + f_1(\theta) = 0,$$

$$f_2''(\theta) + f_2(\theta) = 0,$$

whose general solutions are:

$$f_1(\theta) = A \sin\theta + B\cos\theta, \quad A, B \in \mathbb{R}, \tag{35}$$

$$f_2(\theta) = C \sin\theta + D\cos\theta, \quad C, D \in \mathbb{R}. \tag{36}$$

In conclusion, from (21), (28), (29), (33) and (35)-(36) we have that $\mathbf{w}$ verifies (iii). □

4.2.2. Verification of assumption **(H3)** In three-point bending tests, volume and surface forces are given by the following expressions in cartesian and cylindrical coordinates:

$$\mathbf{f} = -\rho g \mathbf{e}_2 = -\rho g(\sin\theta \mathbf{e}_r + \cos\theta \mathbf{e}_\theta), \tag{37}$$

$$\mathbf{h} = -h\mathbf{e}_2 = -h(\sin\theta \mathbf{e}_r + \cos\theta \mathbf{e}_\theta), \quad h > 0. \tag{38}$$

We are going to prove that these forces satisfy assumption **(H3)** in order to obtain the existence of a unique solution of Problem (VP).

Lemma 2. *In experiment I, volume and surface forces verify assumption* ***(H3)***.

Proof. Taking into account expression (10) and by using (37) and (38), we have

$$\int_\Omega \mathbf{f}\cdot\mathbf{w}\, d\mathbf{x} + \int_{\Gamma_{N_1}} \mathbf{h}\cdot\mathbf{w}\, d\Gamma = -2R(\pi L R \rho g + 2\delta^2 h)A, \tag{39}$$

for every $\mathbf{w} \in \mathbf{R}(\Omega)$ given by *(iii)* of Lemma 1.

Then, hypothesis **(H3)** is verified if we prove that $A \geq 0$, for every $\mathbf{w} \in \mathbf{K}(\Omega) \cap \mathbf{R}(\Omega)$ and $A = 0$ if and only if $w_n = 0$ on Γ_C.

Let us assume that $\mathbf{w} \in \mathbf{K}(\Omega) \cap \mathbf{R}(\Omega)$; since $\mathbf{n} = \mathbf{e}_r$ on Γ_C, we can write

$$w_n = \mathbf{w}\cdot\mathbf{n} = A\sin\theta + B\cos\theta + z(C\sin\theta + D\cos\theta) \leq 0 \text{ a.e. on } \Gamma_C.$$

Consequently:

$$0 \geq \int_{\Gamma_C} \mathbf{w} \cdot \mathbf{n} d\Gamma = -4\hat{\delta} \cos\left(\frac{3\pi}{2} + \frac{\hat{\delta}}{2}\right) RA, \tag{40}$$

and so $A \geq 0$.

In order to complete the proof of **(H3)**, from (40), $A = 0$ if and only if

$$\int_{\Gamma_C} \mathbf{w} \cdot \mathbf{n} d\Gamma = 0.$$

Since $w_n \leq 0$ on Γ_C, we can conclude that $A = 0$ if and only if $w_n = 0$ on Γ_C. □

Lemma 3. *In experiment II, volume and surface forces verify assumption* ***(H3)****.*

Proof. In this case we consider a rectangular domain, where $x_1 \in (-a, a)$, $x_2 \in (-b, b)$ and $x_3 \in (-L, L)$. Let $\mathbf{w} \in \mathbf{K}(\Omega) \cap \mathbf{R}(\Omega)$, we have that

$$\int_{\Omega} \mathbf{f} \cdot \mathbf{w} d\mathbf{x} + \int_{\Gamma_{N_1}} \mathbf{h} \cdot \mathbf{w} d\Gamma = -(8abL\rho g + 4a\delta h)c_2, \tag{41}$$

for every $\mathbf{w} \in \mathbf{R}(\Omega)$ given by *(ii)* of Lemma 1.

Then, hypothesis **(H3)** is verified if we prove that $c_2 \geq 0$, for every $\mathbf{w} \in \mathbf{K}(\Omega) \cap \mathbf{R}(\Omega)$ and $c_2 = 0$ if and only if $\mathbf{w} \in \mathbf{R}_n(\Omega)$.

Let us assume that $\mathbf{w} \in \mathbf{K}(\Omega) \cap \mathbf{R}(\Omega)$; because $\mathbf{w} \cdot \mathbf{n} \leq 0$ *a.e.* on Γ_C, we have that

$$0 \geq \int_{\Gamma_C} \mathbf{w} \cdot \mathbf{n} d\Gamma = -4a\hat{\delta} c_2, \tag{42}$$

and so $c_2 \geq 0$. Moreover, $c_2 = 0$ if and only if

$$\int_{\Gamma_C} \mathbf{w} \cdot \mathbf{n} d\mathbf{x} = 0,$$

and, since the sign of w_n is constant on Γ_C, we conclude that $c_2 = 0$ if and only if $w_n = 0$ on Γ_C. □

4.3. Existence and uniqueness of solution

Proposition 1. *There exists a unique weak solution* $\mathbf{u} \in \mathbf{H}_s^1(\Omega)$ *of Problem* (P)*, defined by (3)-(7), corresponding to experiments I and II for a porcelain beam.*

Proof. Assumptions **(H1)** and **(H6)** are satisfied thanks to expressions (37) and (38). As porcelain is a homogeneous and isotropic material, with positive and constant Lamé parameters, assumption **(H2)** is also verified. Lemmas 2 and 3 guarantee that assumption **(H3)** is satisfied for experiments I and II, respectively. Assumption (H5) is also verified due to the sample geometries.

Furthermore, it is easy to verify assumption **(H4)**. Indeed, if we consider $\mathbf{w} \in \mathbf{K}(\Omega) \cap \mathbf{R}(\Omega)$,

$$\mathbf{w} \cdot \mathbf{n} = (c_1 + d_2 x_3 - d_3 x_2) n_1 + (c_2 + d_3 x_1 - d_1 x_3) n_2 \leq 0 \text{ on } \Gamma_C.$$

Finally, since n_2 is non null, choosing $c_1 = d_2 = d_3 = 0$ and $c_2, d_1 \neq 0$, we obtain that there exists $\mathbf{w} \in (\mathbf{K}(\Omega) \cap \mathbf{R}(\Omega)) \setminus \mathbf{R}_n(\Omega)$, $\mathbf{w} \neq \mathbf{0}$, such that

$$\mathbf{w} \cdot \mathbf{n} = (c_2 - d_1 x_3) n_2 \neq 0.$$

So the result is obtained from Theorem 1. □

5. Obtaining a new formula for the MOR

In [3], we have obtained the one-dimensional variational problems associated to the bending and axial displacements in three-point bending tests by applying the well-known method of asymptotic expansions. We have proved that a good approximation of the solution of the three-dimensional Problem (VP) is the limit displacement $\mathbf{u}^0 = (u_1^0, u_2^0, u_3^0)$, where the transversal displacement, u_1^0, is null, the bending displacement, u_2^0, only depends on x_3, and the axial displacement, u_3^0, is given by:

$$u_3^0 = \underline{u}_3^0 - x_2 \partial_3 u_2^0. \tag{43}$$

In particular, we have proved that the bending and axial displacements are the solution of the following variational problems:

Problem $(\mathbf{P}_2^0)$:

Find $u_2^0 \in H_e^2(-L, L)$, such that $u_2^0 \geq 0$ in $\Gamma_C^0 = (-I - \hat{\delta}, -I) \cup (I, I + \hat{\delta})$ and

$$\int_{-L}^{L} EI_1 \Delta u_2^0 \Delta(v_2^0 - u_2^0) dx_3 \geq \int_{-L}^{L} q_2 (v_2^0 - u_2^0) dx_3, \tag{44}$$

for all $v_2^0 \in H_e^2(-L,L)$ such that $v_2^0 \geq 0$ in Γ_C^0. Here, $H_e^2(-L,L)$ is the subspace of even functions in $H^2(-L,L)$ and q_2 is the total vertical force per unit of length:

$$q_2(x_3) = -\rho g \beta - \chi_{(-\delta,\delta)}(x_3)\alpha h,$$

where:

$$\beta = \begin{cases} \pi R^2 & \text{for experiment I} \\ 4ab & \text{for experiment II} \end{cases}, \quad \alpha = \begin{cases} 2\delta R & \text{for experiment I} \\ 2a & \text{for experiment II.} \end{cases}$$

Problem $(\mathbf{P}_3^0)$:
Find $\underline{u}_3^0 \in H_o^1(-L,L)$, such that

$$\int_{-L}^{L} \partial_3 \underline{u}_3^0 \, \partial_3 v_3^0 dx_3 = 0, \; \forall v_3^0 \in H_o^1(-L,L), \tag{45}$$

where $H_o^1(-L,L)$ is the subspace of odd functions in $H^1(-L,L)$.

In [3], we have also established some properties of the bending and axial displacements which are collected in the following propositions.

Proposition 2. *In the scenario of experiments I and II, the bending and axial problems* $(\mathbf{P}_2^0)$ *and* $(\mathbf{P}_3^0)$ *have unique solutions. Furthermore,* $\underline{u}_3^0$ *is null and the axial normal stress is given by the expression*

$$\sigma_{33}^0(\mathbf{x}) = -E x_2 \Delta u_2^0(x_3), \; \forall \mathbf{x} \in \Omega. \tag{46}$$

Proposition 3. *Let denote the coincidence set*

$$I = \{x_3 \in \overline{\Gamma}_C^0; u_2^0(x_3) = 0\}.$$

i) The bending displacement u_2^0 *satisfies the following differential problem:*

$$E I_1 \Delta^2 u_2^0 = q_2 + \mu \text{ in } (-L,L), \tag{47}$$

$$\partial_3 \Delta u_2^0(\pm L) = \Delta u_2^0(\pm L) = 0, \tag{48}$$

where μ *is a nonnegative Radon measure* μ *such that* $\text{supp}(\mu) \subset I$.

ii) u_2^0 *verifies the regularity properties:*

$$u_2^0 \in \mathcal{C}^2(-L,L) \cap \mathcal{C}^3((-L,L)\backslash I). \tag{49}$$

iii) The lateral limits $\partial_3 \Delta u_2^0(x_3^{\pm})$ *exist for all* $x_3 \in I$ *and*

$$\partial_3 \Delta u_2^0(x_3^+) \geq \partial_3 \Delta u_2^0(x_3^-), \forall x_3 \in I.$$

iv) The measure μ *verifies:*

$$\mu(I) = -\int_{-L}^{L} q_2 dx_3. \tag{50}$$

v) The reciprocal of i) is also true if $u_2^0 \geq 0$ *in* Γ_C^0.

In the particular case of the experiments I and II, we can demonstrate that the effective support on each lower cylinder will be a point or an interval.

Proposition 4. *Let* u_2^0 *be the solution of Problem* $(\mathbf{P}_2^0)$. *If* x_0, $x_1 \in I$ *with* $0 < x_0 < x_1$, *therefore* $[-x_1,-x_0] \cup [x_0,x_1] \subset I$.

Proof. The proof is very close to that given in [9]. From now on, we denote $\tilde{I} = [-x_1,-x_0] \cup [x_0,x_1]$. We define the following function:

$$v = u_2^0(1 - \chi_{\tilde{I}})$$

which satisfies $v \in H_e^2(-L,L)$ as a straightforward consequence of the fact that $u_2^0 \in H_e^2(-L,L) \subset \mathcal{C}^1(-L,L)$ and $u_2^0 \geq 0$ on Γ_C^0. Moreover, $v \geq 0$ in Γ_C^0.

We consider $w = u_2^0 - v \in H_e^2(-L,L)$ that verifies $w \geq 0$ on $\tilde{I}$ and $w = 0$ on $(-L,L)\backslash\tilde{I}$. Then, choosing $v_2^0 = w + u_2^0$ as test function in expression (44), we have that

$$\int_{-L}^{L} E I_1 \Delta u_2^0 \Delta w dx_3 \geq \int_{-L}^{L} q_2 w dx_3,$$

and from the definition of w,

$$\int_{\tilde{I}} EI_1 \Delta u_2^0 \Delta u_2^0 dx_3 \geq \int_{\tilde{I}} q_2 u_2^0 dx_3.$$

Now, choosing $v_2^0 = v$ as test function in expression (44), we have that

$$\int_{-L}^{L} EI_1 \Delta u_2^0 \Delta (v - u_2^0) dx_3 \geq \int_{-L}^{L} q_2 (v - u_2^0) dx_3,$$

and taking into account the definition of v,

$$\int_{\tilde{I}} EI_1 \Delta u_2^0 \Delta u_2^0 dx_3 \leq \int_{\tilde{I}} q_2 u_2^0 dx_3.$$

Therefore, we deduce that

$$0 \leq \int_{\tilde{I}} EI_1 \Delta u_2^0 \Delta u_2^0 dx_3 = \int_{\tilde{I}} q_2 u_2^0 dx_3 \leq 0, \tag{51}$$

since q_2 is negative and u_2^0 positive. Relation (51) implies that $\Delta u_2^0 = 0$ in $\tilde{I}$ and as $u_2^0 = 0$ in $\partial\tilde{I}$, then $u_2^0 = 0$ on $\tilde{I}$ and we conclude the proof. □

Corollary 1. *The coincidence set I is either two isolated points or two closed intervals.*

5.1. Analytical solution. A new formula for MOR

It is easy to obtain an analytical solution of differential problem (47)-(48):

Proposition 5. *An analytical solution of differential problem (47)-(48) is given by:*

$$u_2^0(x_3) = \frac{1}{24EI_1} \begin{cases} -(\alpha h + \rho g \beta) x_3^4 + b_3 x_3^2 + d_3 \text{ in } (-\delta, \delta), \\ -\rho g \beta (x_3^4 - I^4) + b_2 (x_3^3 - I^3) + c_2 (x_3^2 - I^2) + d_2 (x_3 - I) \text{ in } [\delta, I), \\ -\rho g \beta (x_3^4 - I^4) + b_1 (x_3^3 - I^3) + c_1 (x_3^2 - I^2) + d_1 (x_3 - I) \text{ in } [I, L), \end{cases}$$

and by its even extension in $[-L, -\delta)$, where

$$\begin{aligned} &b_1 = 4\rho g \beta L, \quad b_2 = -4\alpha h \delta, \quad b_3 = 6\rho g \beta L(2I - L) - 6\alpha h \delta(\delta - 2I), \\ &c_1 = -6\rho g \beta L^2, \quad c_2 = 6\rho g \beta L(2I - L) + 12\alpha h \delta I, \\ &d_1 = 12\rho g \beta L I^2 - 4\alpha h \delta(\delta^2 - 3I^2), \quad d_2 = -4\alpha h \delta^3, \\ &d_3 = \rho g \beta I^2 \left(I^2 - 6L(2I - L)\right) - \alpha h \delta(8I^3 + \delta^3 - 4\delta^2 I). \end{aligned}$$

The Radon measure μ is given by:

$$\mu = (\alpha h \delta + \rho g \beta L)(\delta_{\{x_3 = -I\}} + \delta_{\{x_3 = I\}}), \tag{52}$$

and $I = \text{supp}(\mu) = \{-I, I\}$.

Moreover, the axial normal stress σ_{33}^0 on each transversal section of the beam is expressed by:

$$\sigma_{33}^0(\mathbf{x}) = \frac{x_2}{2I_1} \begin{cases} \rho g \beta (x_3^2 + L^2 - 2LI) + \alpha h (x_3^2 + \delta^2 - 2\delta I), & \text{if } x_3 \in (-\delta, \delta), \\ \rho g \beta (x_3^2 + L^2 - 2LI) + 2\alpha h \delta (x_3 - I), & \text{if } x_3 \in (\delta, I) \\ \rho g \beta (L - x_3)^2, & \text{if } x_3 \in (I, L). \end{cases} \tag{53}$$

Proof. It is easy to check that u_2^0 is a solution of equation (47) with μ given by expression (52). So, the proof is a straightforward consequence from Proposition 3. □

Figures 3 and 4 show a graphical representation of the analytical solution of Problem (47)-(48) for the experiment II with the following data:

$$\begin{aligned} &2L = 0.118\text{m}, \ 2a = 2b = 0.0085\text{m}, \ 2l = 0.06\text{m}, \ \delta = 0.0025\text{m}, \\ &E = 6.9975 \times 10^{10}\text{N/m}^2, \ \rho = 2340\text{kg/m}^3, \ h = 5649412\text{N/m}^2. \end{aligned}$$

These values will be used both in the experiments in laboratory and in the numerical simulations. Notice that the second derivative of u_2^0 is still continuous while in the third derivative there exist two discontinuities in the support points, $\pm I$, which conform the coincidence set I.

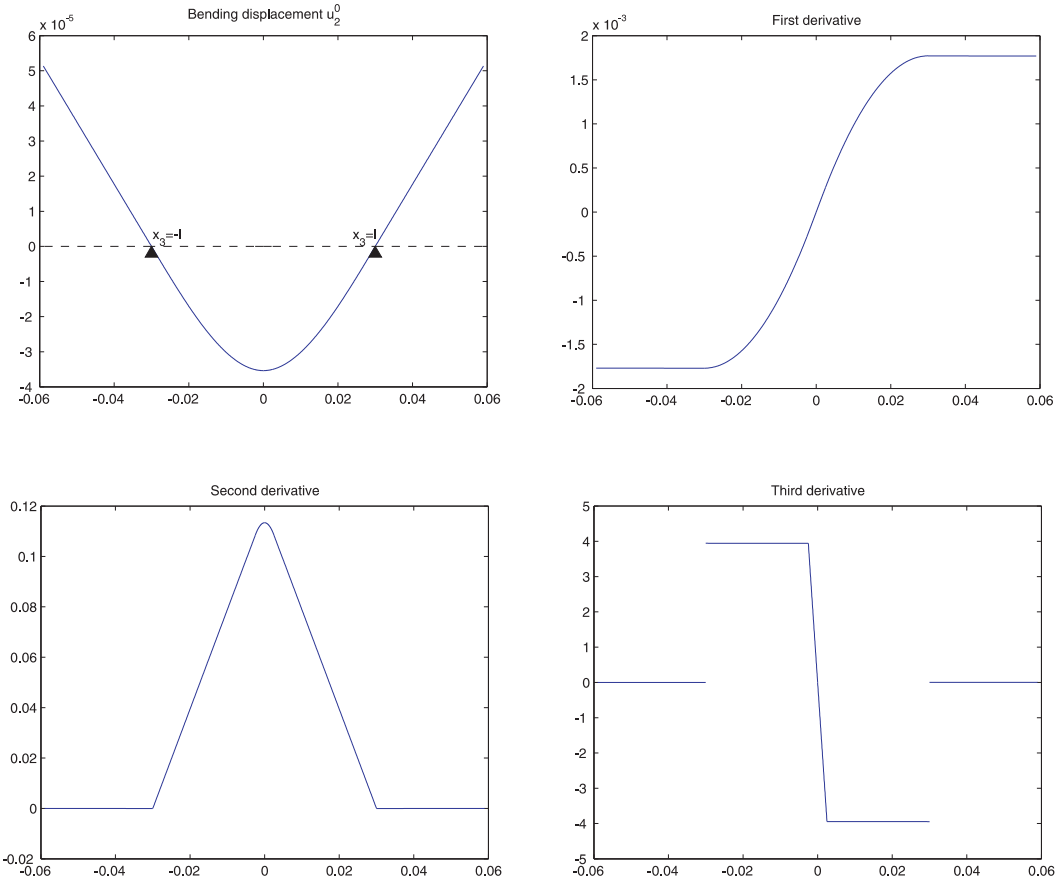

Figure 3. Analytical solution of Problem (47)-(48) and its derivatives.

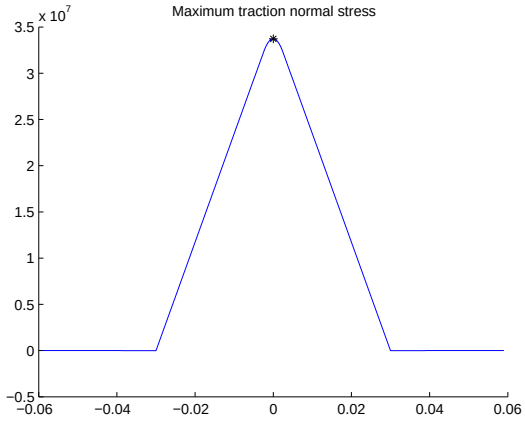

Figure 4. Axial normal stress obtained in the fiber $x_2 = -b$.

Corollary 2. *i) If the following condition is satisfied:*

$$\rho g \beta l \left(3(L-l)^2 - 2l^2\right) - \alpha h \delta (3l^2 - \delta^2) < 0, \tag{54}$$

then, there exists $\hat{\delta}_0 > 0$ such that for all $\hat{\delta} < \hat{\delta}_0$ the analytical solution given in Proposition 5 is the unique solution of variational problem $(\mathbf{P}_2^0)$.

ii) If condition (54) is satisfied and $\hat{\delta}$ verifies

$$\rho g\beta\left[(2l+\hat{\delta})((l+\hat{\delta})^2+l^2+6L^2)-4L((2l+\hat{\delta})(l+\hat{\delta})+4l^2)\right]-4\alpha h\delta(3l^2-\delta^2)<0. \tag{55}$$

then, u_2^0 is the unique solution of variational problem $(\mathbf{P}_2^0)$.

Proof. i) Condition (54) guarantees that $\partial_3 u_2^0(l)>0$, so there exists $\hat{\delta}_1>0$ such that u_2^0 is increasing in $(l, l+\hat{\delta}_1)$. Moreover, since $u_2^0(l)=0$, we deduce that u_2^0 is positive in the interval $(l, l+\hat{\delta})$, with $\hat{\delta}<\hat{\delta}_0=\min(\hat{\delta}_1, L-l)$. A similar argument can be used at $x_3=-l$. Therefore, u_2^0 is the solution of Problem $(\mathbf{P}_2^0)$.

ii) Condition (55) guarantees that the solution is positive at $x_3=l+\hat{\delta}$. Thanks to condition (54) and taking into account that u_2^0 is a concave function in the interval (l, L), we can state that u_2^0 is positive in the interval $(l, l+\hat{\delta})$.

□

From expression (53), we can deduce a new formula for the MOR. Recall that the MOR corresponds with the maximum surface stress of the bent beam at the instant of failure. As we will see, the maximum stress occurs in the opposite zone to the load application zone, which coincides with the results found in the classic literature.

Proposition 6. *If $2l>L$, then the maximum fiber normal stresses are achieved at $(0,\pm d,0)$ and their values are:*

$$\sigma_{mt}=\frac{d}{2l_1}\left[\alpha h\delta\,(2l-\delta)-\rho g\beta L(L-2l)\right], \tag{56}$$

for the maximum in traction and

$$\sigma_{mc}=-\sigma_{mt},$$

for the maximum in compression, where d is the farthest distance in the x_2-direction from the axis of the beam.

Proof. Let us suppose that x_2 is fixed and let us define

$$f(x_3)=\sigma_{33}^0(x_2,x_3),$$

with σ_{33}^0 defined by (53). Then,

$$\frac{df}{dx_3}(x_3)=\frac{x_2}{l_1}\begin{cases}x_3(\rho g\beta+\alpha h), & \text{if } x_3\in(-\delta,\delta),\\ \rho g\beta x_3+\alpha h\delta, & \text{if } x_3\in[\delta,l)\\ -\rho g\beta(L-x_3), & \text{if } x_3\in(l,L],\end{cases}$$

In order to study the extrema of f we have to analyze its critical points $x_3=0$, $x_3=\pm L$ and also the jump discontinuities of its derivative $x_3=\pm l$. So, we can distinguish two situations:

i) If $x_2<0$, we have that $x_3=0$ is a local maximum that verifies:

$$f(0)>0=f(\pm L),$$

if $2l>L$. Furthermore, $f(\pm l)\le 0$, so the maximum traction normal stress is achieved at $(0,-d,0)$.

ii) Analogously if $x_2>0$, we have that $x_3=0$ is a local minimum that verifies:

$$f(0)<0=f(\pm L),$$

if $2l>L$. Furthermore, $f(\pm l)\ge 0$, so the maximum compression normal stress is achieved at $(0,d,0)$.

□

Corollary 3. *The MOR for the experiment I is given by*

$$\sigma_{ft}^0=\frac{H}{\pi R^3}(2l-\delta)-\frac{F}{\pi R^3}(L-2l). \tag{57}$$

where F and H are the modulus of the total gravity forces and the load of failure, respectively. Analogously, the MOR for the experiment II is given by

$$\sigma_{ft}^0=\frac{3H}{16ab^2}(2l-\delta)-\frac{3F}{16ab^2}(L-2l). \tag{58}$$

Proof. From expression (56) and taking into account that

$$I_1 = \frac{\pi R^4}{4},\ I_1 = \frac{4}{3}ab^3,$$

for experiments I and II, respectively, we have that

$$\sigma_{mt} = \frac{2}{\pi R^3}\left[\alpha h\delta\,(2l-\delta) - \rho g\beta L(L-2l)\right] \text{ for experiment I,}$$
$$\sigma_{mt} = \frac{3}{8ab^2}\left[\alpha h\delta\,(2l-\delta) - \rho g\beta L(L-2l)\right] \text{ for experiment II.}$$

Then, since the total gravity forces and the load of failure are given by

$$F = 2L\rho g\beta,\ H = 2\delta\alpha h,$$

we conclude the proof. □

Notice that if the total gravity forces, F, can be neglected and the upper cylinder exerts really a punctual force, that is $\delta = 0$, expressions (57) and (58) are in line with classic formulae (1) and (2). Here, the parameter δ is related to the contact area between the upper cylinder exerting the load and the deflected beam. In the case of rectangular beams, this contact area is easily to be determined as a function of the load H. In the case of cylindrical beams, this area is more difficult to compute but an estimation can be considered to determine the parameter δ.

6. Computing the MOR.

In this section we are going to show the results from numerical simulations of experiments I and II described in Section 6. These experiments have been carried out in collaboration with the Institute of Ceramics of the Universidade de Santiago de Compostela.

In this section, the methodology to compute the MOR is as follows:

- Firstly, we have carried out various laboratory tests on porcelain beams in order to determine the experimental force of rupture, **H**.
- Secondly, we calculate a theoretical value for the modulus of rupture, σ_{ft}, by using the classic formulas of the MOR (1) and (2).
- Thirdly, considering the experimental force of rupture, **H**, we compute numerically the corresponding three-dimensional stresses and so, we compute its 3d numerical MOR, σ_{fn}.
- Fourthly, we compute numerically the displacements and stresses by using the one-dimensional model and, therefore, we compute its 1d numerical MOR, σ^0_{fn}.
- Finally, we also compute a new value for the MOR, the 1d analytical MOR, denoted by σ^0_{ft}, by using expressions (57) and (58) obtained in previous Section.

These all experiences are repeated for different sizes of samples and for different distances between the two lower cylinders.

In order to carrying out the three-dimensional numerical simulations that we present below we use the finite element software package MSC.MARC†, that let us make simulations in solids mechanics when there exist contact conditions with a foundation or a deformable body. We show below figures corresponding to the computed stresses and displacements, and tables with computed values for the MOR, by using hexahedrical meshes with a characteristic size of $e = 0.0025\,\text{m}$. Besides, for the one-dimensional numerical simulation, a MATLAB code has been developed which uses a generalized Newton technique to deal with the nonlinearity due to the contact conditions (see [10]).

In our experiments, the beams are made of porcelain, a brittle material which breaks suddenly, when the response is still substantially elastic and linear. In material databases, the characteristic parameters of porcelain range between the following values:

$$E = 6.82\times10^{10} - 7.175\times10^{10}\,\text{N/m}^2,$$
$$\nu = 0.17 - 0.18,$$
$$\rho = 2260 - 2420\,\text{kg/m}^3.$$

The characteristic parameters of porcelain we use in the numerical simulations are the following:

$$E = 6.9975\times10^{10}\,\text{N/m}^2, \nu = 0.175,\ \rho = 2340\,\text{kg/m}^3.$$

†MSC.MARC is a registered trademark of MSC.Software Corporation.

6.1. Numerical results for Experiment I

As we have said above, in experiment I we use cylindrical beams of radius $R = 0.009\,\text{m}$ and we consider two lengths:

$$2L_1 = 0.125\,\text{m},\ 2L_2 = 0.18\,\text{m}.$$

For each fixed length, three different distances between the two lower cylinders are considered:

$$2l_1 = 0.06\,\text{m},\ 2l_2 = 0.1\,\text{m},\ 2l_3 = 0.15\,\text{m}.$$

The parameters δ and $\hat{\delta}$ are taken as 0.0025.

Table 1 shows the modulus of the maximum surface stress of the bent beams at the instant of failure. These values were obtained by making several laboratory tests, and taking the arithmetic mean of the corresponding rupture loads. Notice that the experimental rupture load varies substantially with the dimensions of the beam, depending on the relation between the total length and the distance between the two lower cylinders.

With the values for the rupture loads of Table 1 and by using the classic formula (1), we obtain theoretical values for the MOR, denoted by σ_{ft}, which are different with each sample (see Table 2).

Next, we are going to compute the MOR by means of three-dimensional numerical simulations and by using again the values of the experimental rupture loads, we solve the problem numerically. Figure 5 shows the vertical displacement and the x_3x_3 component of the stress tensor for a particular sample. Notice that the greatest deflection appears in the center of the beam, while the smallest displacements occur in the contact boundary. Moreover, it is also important to notice that the behaviour of the beam is almost constant at each cross section. We can also observe that the greatest value of the stresses in compression is reached in the force application zone, while the greatest value in bending appears in the opposite zone, in which the beam collapses. Table 3 shows the maximum value of the x_3x_3 component of the stresses at this zone for each sample. This value is denoted in the following by σ_{fn}, the 3d numerical value for the MOR.

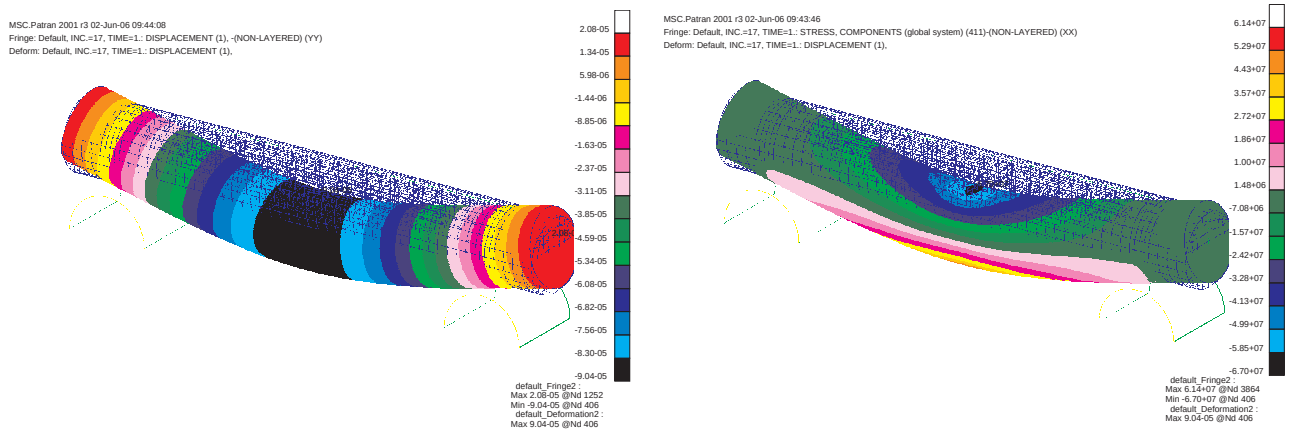

Figure 5. Vertical displacement and x_3x_3 component of stresses for a cylindrical beam with $2L_1 = 0.125\text{m}$ and $2l_2 = 0.1\text{m}$.

By using the one-dimensional bending problem (44) we carry out a new numerical simulation of the three-point bending test, obtaining in this way a 1d numerical approach for the MOR, denoted by σ^0_{fn}. This new value for the MOR has a great importance to compute the MOR for brittle materials, because the three-dimensional simulations can be inaccurate when the ratio between the area of the cross-section and the length of the beam is very small.

In Figures 6 and 7, the bending displacement u_2 and the axial normal stress σ_{33} for a porcelain beam obtained from the one and three-dimensional numerical simulations are shown as well as the 1d analytical solution obtained in Section 5.1. In these figures, the plots on the right represent a zoom of the axial normal stress in order to better appreciate the behaviour in the loading area; moreover, the theoretical MOR and the 3d and 1d numerical MOR are also depicted. These values are computed in the maximum deflection line, that is, in $x_2 = -R$.

Notice that when comparing Figures 6.b) and 7.b) for the same distance between the two lower cylinders, the smaller the ratio between the area of the cross-section and the length of the beam is, the better the 1d numerical MOR approaches the theoretical MOR. Furthermore, we can observe that the 1d numerical MOR comes closer to the theoretical MOR when the distance between the two lower cylinders becomes larger, while the approach is worse when the two lower cylinders are nearer.

Finally, the last approach for the MOR is obtained by using the new expression (57) arising from the analytical solution we have calculated from the asymptotic analysis of the problem, called the 1d analytical MOR and denoted by σ^0_{ft} (this value is also shown in Figures 6 and 7). Tables 4 and 5 gather the different values obtained for the MOR of a cylindrical beam of porcelain. Notice that, the differences decrease when the two lower cylinders are close to the ends of the beam; so, the theoretical expression (1) gives a good approach when the beam is supported at its ends.

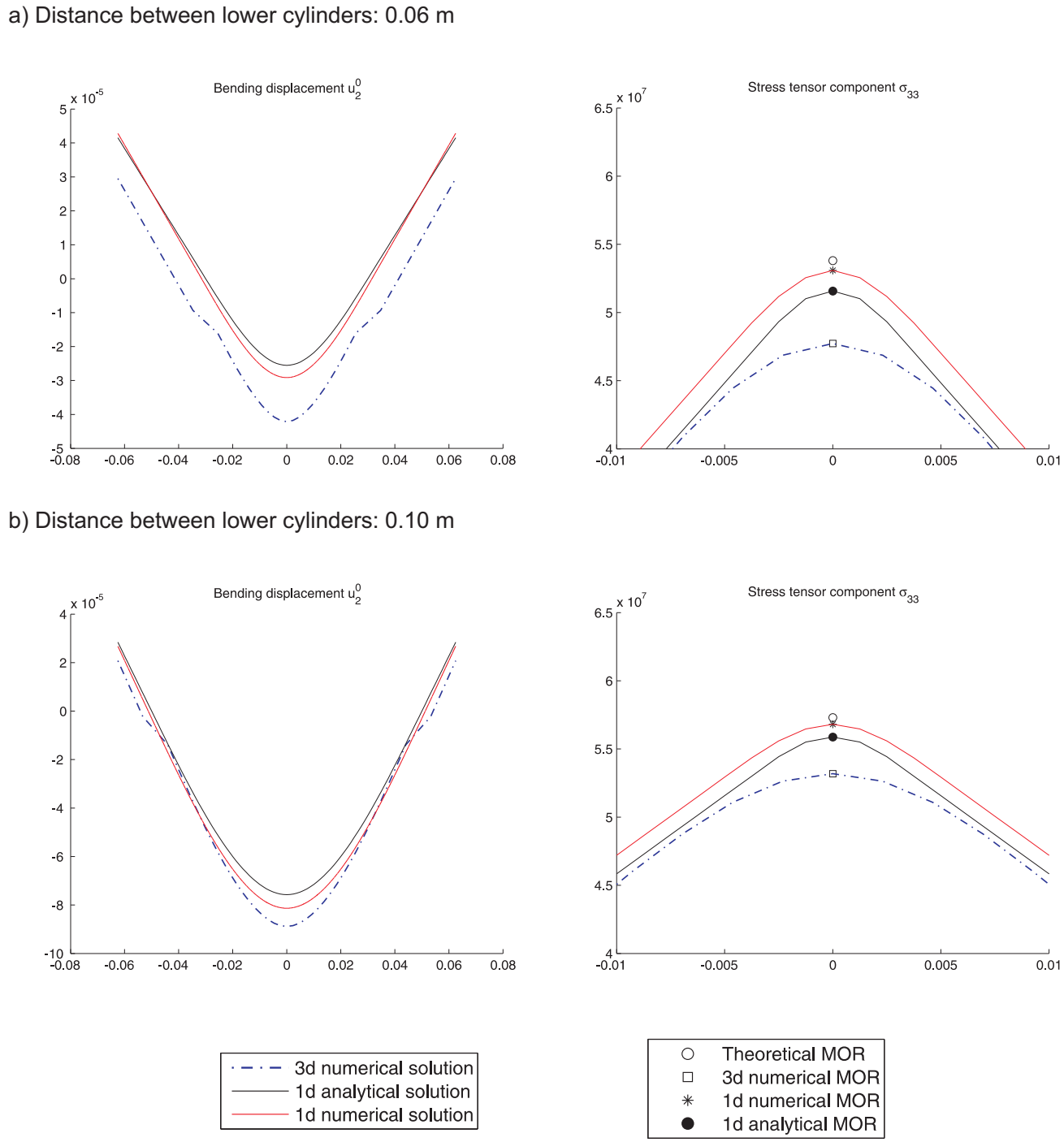

Figure 6. Bending displacement and axial normal stress for a cylindrical beam with $2L_1 = 0.125$m.

6.2. Numerical results for Experiment II

In experiment II, we use beams of square section, of height and width $2a = 2b = 0.0085\,\text{m}$ and of length $2L = 0.118\,\text{m}$. The distances between the two lower cylinders considered are $2l_1 = 0.06\,\text{m}$ or $2l_2 = 0.1\,\text{m}$. Again, the parameters δ and $\hat{\delta}$ have the same value, that is, 0.0025.

Table 6 shows the modulus of the experimental load at the instant of failure and the corresponding theoretical MOR, σ_{ft}, obtained from the classic formula (2).

Following the same procedure as in the cylindrical case, firstly, we carried out the three-dimensional numerical simulations corresponding to the experimental rupture loads obtained in laboratory. Figure 8 shows the vertical displacement and the x_3x_3

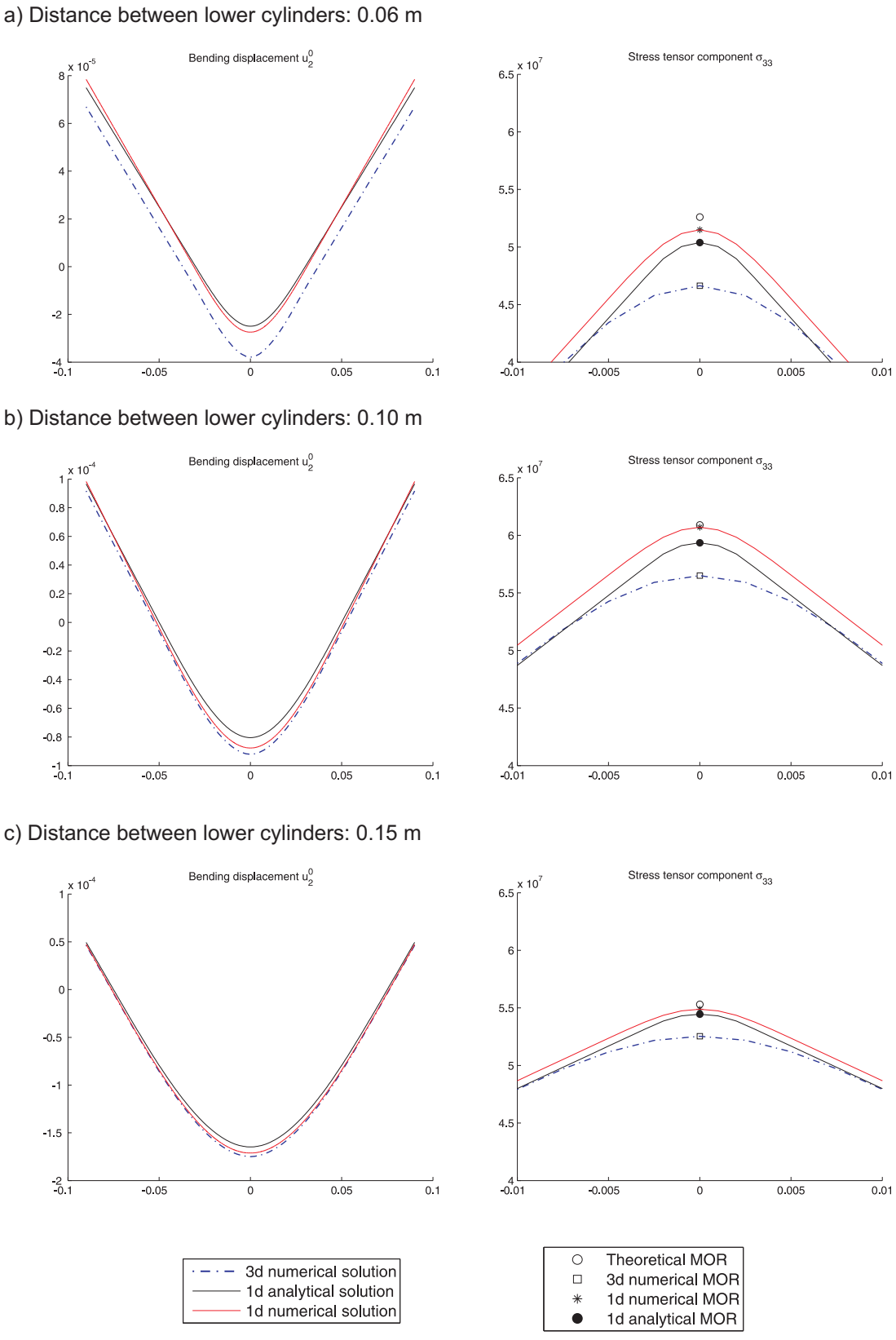

Figure 7. Bending displacement and axial normal stress for a cylindrical beam with $2L_1 = 0.18$m.

component of the stress tensor for a particular sample. In column 3 in Table 7 we show the 3d numerical MOR of porcelain, σ_{fn}.

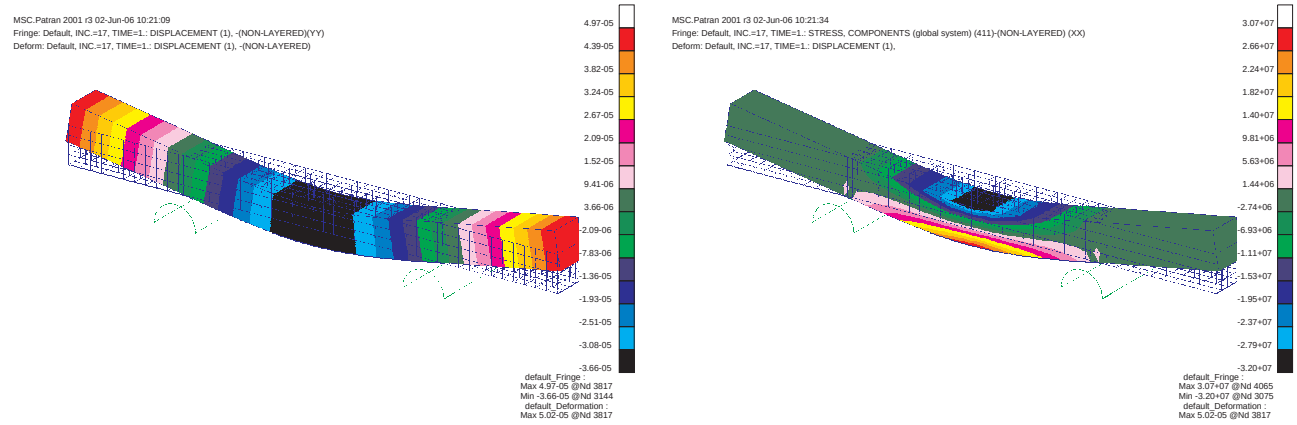

Figure 8. Vertical displacement and x_3x_3 component of stresses for a beam of square section with $2L = 0.118$m and $2l = 0.06$m.

Again, by using the one-dimensional bending problem (44) we carry out a new numerical simulation of the three-point bending test, to obtain the 1d numerical MOR, σ^0_{fn} (see Column 4 in Table 7).

In Figure 9 the bending displacement, u_2, and the axial normal stress, σ_{33}, for a porcelain beam, obtained from the one and three-dimensional numerical simulations are shown as well as the 1d analytical solution obtained in Section 5.1. As we have done above, the plots on the right represent a zoom of the axial normal stress to better appreciate the behaviour in the loading area. Moreover, the theoretical and the 1d and 3d numerical MOR are depicted. These values are computed in the maximum deflection line, that is, in $x_2 = -b$.

Finally, the 1d analytical MOR, σ^0_{ft}, is obtained by using the expression (58) arising from the asymptotic analysis of the problem (this value is also shown in Figure 9). Table 7 gathers the different values obtained for the MOR of a porcelain beam of square section. Notice that, as in the experiment I, the differences are smaller when the two lower cylinders are close to the ends of the beam, showing that the theoretical expression (2) gives a good approach when the beam is supported at its ends.

7. Conclusions

In this work, we have carried out a complete analysis of the MOR for brittle materials, and comparing four different methodologies to obtain an approach of its value. We have proved that the assumptions of compatibility on the forces introduced in [3] are satisfied for laboratory three-point bending tests with cylindrical and square beams. These hypotheses are necessary to guarantee the existence of a unique solution of the problem due to the absence of Dirichlet conditions. Moreover, thanks to the one-dimensional problems obtained using the asymptotic expansion method, we have deduced a new expression for the MOR, which involves not only the rupture load and the distance between the two lower cylinders but also the gravitational effects and the distance between the supports and the ends of the beam.

In order to find an effective method to compute the MOR of brittle materials, we have carried out a comparison between four methodologies applied to cylindrical and square beams: Firstly, we have experimentally measured the rupture load at the instant of failure at laboratory. By using the classical formulas (1) and (2), we have computed the corresponding theoretical MOR. Secondly, from the numerical simulations we have obtained the 3d and 1d numerical MOR. Finally, by using the new expressions obtained in this work by means of the one-dimensional analytical solution, we have computed a new 1d analytical MOR. After comparing all the values obtained, we conclude that formulas (57) and (58) give a better approach of the MOR for brittle materials than the classical ones. Moreover, we want to remark that the MOR for brittle materials is a mechanical property strongly sensitive to variations in the dimensions of the beam; due to this, we have found that there exist great differences between the values for the MOR obtained in this work and the range of values found in databases in which the dimensions or the geometries of the samples are not indicated.

8. Acknowledgments

This research was supported by FEUGA (projects 2001/CE230, 2002/CG428), CICYT-FEDER (projects DPI2001-2908, DPI2004-01993, MTM2008,05682) and Xunta de Galicia (project PGIDIT05PXIC20701PN).

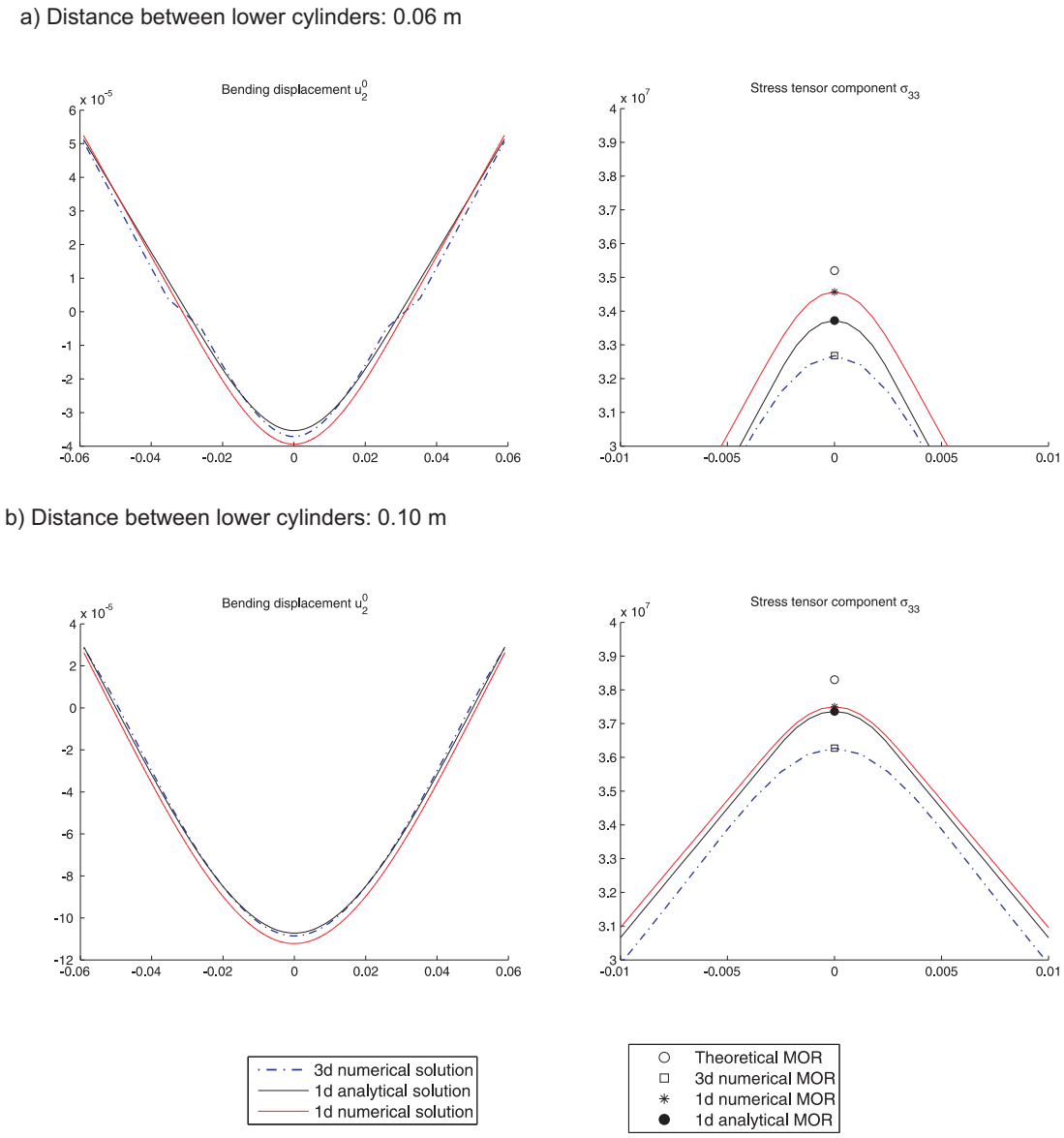

Figure 9. Bending displacement and axial normal stress for a beam of square section with $2L_1 = 0.118$m.

Appendix A: Modulus of rupture

This appendix offers a basic explanation of the expression for the MOR of a material obtained by using habitual procedures in solid mechanics. In addition, using physical hypotheses, we will deduce the classical formula for the MOR. A more detailed description of this can be found in [11, 12, 13].

In engineering science, three-point bending tests are generally used to determine the MOR of materials: The value corresponding to the maximum surface stress that the beam supports until breaking. Compressive stresses are generated on the upper surface while bending stresses occur on the lower surface. The fracture generally starts on the lower surface, and the maximum bending stress is produced on the region opposite to the loading area, where the upper cylinder applies surface forces.

The classical formula for the MOR we consider in this article is obtained from the stresses generated in a beam subjected to pure bending, that is, when the bending moment is constant. A clear example of pure bending is a beam subjected to two pairs M of the same direction and magnitude but acting on opposite directions at the ends of the beam. This configuration produces a constant bending moment M over the entire length of the beam. A three-point bending test, however, is an example of non uniform bending: the bending moment varies along the length of the beam. Despite this difference between bending moments, the classic mechanical bibliography, based on Saint Venant's principle, considers that the experimental results obtained for pure bending can also be used for non uniform bending.

In pure bending, the following bending stress formula is obtained (see [11]):

$$\sigma_{33} = -\frac{Mx_2}{I_1}, \tag{59}$$

which shows that stresses are directly proportional to the bending moment M and to the coordinate x_2, and inversely proportional to the second moment of inertia, I_1, of the transversal section of the beam. The maximum bending or compression stresses are produced at points placed at the farthest distance from the axis of the beam denoted by d_1 and d_2, above and below the beam, respectively. The corresponding maximum stresses are

$$\sigma_{33_1} = -\frac{Md_1}{I_1}, \quad \sigma_{33_2} = \frac{Md_2}{I_1}.$$

The second expression is the classical formula for the MOR when the bending moment is constant.

In three-point bending tests there exists non uniform bending moment, that is, M is not constant. Therefore, in order to give the classical expression for the MOR when a beam is subjected to this test, we must determine the maximum bending moment, M_{max}. Consequently, the MOR would be given by the expression

$$\sigma_f = \frac{M_{max}d_2}{I_1}, \tag{60}$$

where $d_2 > 0$ denotes the distance from the axis of the beam to its boundary in the negative direction x_2.

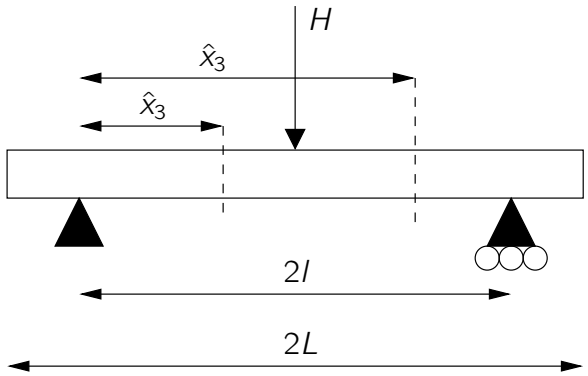

Figure 10. Simply supported beam subjected to a concentrated force H.

To compute M_{max}, we consider a beam of length $2L$, that is simply supported at points placed at a distance $2l$ and is subjected to a concentrated load H in its center (see Fig. 10). If we consider this beam like a free body, we can determine easily the reactions in the beam from the moment equilibrium equation, that is:

$$R_{-l} = R_l = \frac{H}{2}.$$

We cut the beam in a section to the left of the load H and at a distance $\hat{x}_3$ from the support in $x_3 = -l$. From the equilibrium equation for this free body, we obtain that the bending moment at a distance $\hat{x}_3$ from the left support is

$$M = R_{-l}\hat{x}_3 = \frac{H\hat{x}_3}{2}, \quad 0 < \hat{x}_3 < l.$$

Analogously, if we cut the beam in a section to the right of the load H and at a distance $\hat{x}_3$ from the support in $x_3 = -l$, we obtain that the bending moment is

$$M = R_{-l}\hat{x}_3 - H(\hat{x}_3 - l) = \frac{H\hat{x}_3}{2} - H(\frac{\hat{x}_3}{2} - l) = \frac{H}{2}(2l - \hat{x}_3), \quad l < \hat{x}_3 < 2l.$$

Therefore, the bending moment for a simply supported beam in a point placed at a distance $\hat{x}_3$ from the left support is

$$M = \begin{cases} \frac{H\hat{x}_3}{2}, & 0 < \hat{x}_3 < l, \\ \frac{H}{2}(2l - \hat{x}_3), & l < \hat{x}_3 < 2l. \end{cases}$$

The maximum bending moment is

$$M_{max} = \frac{Hl}{2}, \tag{61}$$

and is produced under the concentrated load H in $\hat{x}_3 = l$.

Substituting (61) in (60), we obtain that the classical expression for the MOR of a material is

$$\sigma_f = \frac{M_{max}d_2}{I_1} = \frac{Hld_2}{2I_1}.$$

References

1. Chung KH, Lee W, Kim JH, Kim C, Park SH, Kwon D, Chung K. Characterization of mechanical properties by indentation tests and FE analysis - validation by application to a weld zone of DP590 steel. *International Journal of Solids and Structures*. 2009; 46: 344–363.
2. Borg SF. *Matrix-Tensor Methods in Continuum Mechanics*. World Scientific: Singapore; 1990.
3. Quintela P, Sánchez MT. Three-point bending tests. Part I: Mathematical study and asymptotic analysis. Submitted to publication in *Mathematical Methods in the Applied Sciences*.
4. Kikuchi N, Oden JT. *Contact problems in elasticity: a study of variational inequalities and finite element methods*. SIAM: Philadelphia; 1988.
5. Fichera G. Problemi elastostatici con vincoli unilateri: il problema di Signorini con ambigue condizioni al contorno. *Atti della Accademia Nazionale dei Lincei. Memorie. Serie 8*. 1964; 7: 91-140.
6. Duvaut G. *Mécanique des milieux continus*. Masson: Paris; 1990.
7. Nečas J, Hlaváček I. *Mathematical Theory of Elastic and Elastico-Plastic Bodies: An Introduction*. Elsevier Scientific: Amsterdam; 1981.
8. Henry JP, Parsy F. *Cours d'Elasticité*. Dunod: Paris; 1982.
9. Cimatti G. The constrained elastic beam.*Meccanica (8)*. 1973; 2:119–124.
10. Barral P, Moreno C, Quintela P, Sánchez MT. A numerical algorithm for a Signorini problem associated with Maxwell-Norton materials by using generalized Newton's methods, *Comput. Methods Appl. Mech. Engrg.* 2006; 195: 880–904.
11. Beer FP, Johnston ER. *Mechanics of Materials*. McGraw-Hill: New York; 1992.
12. Gere JM, Timoshenko SP, *Mecánica de materiales*. International Thomson Editores: Mexico; 1998.
13. Seed GM. *Strength of Materials. An undergraduate text*. Saxe-Coburg: Edinburgh; 2000.

Table 1. Experimental load of failure for cylindrical beams.

$2L$ / $2l$	$2l_1 = 0.06\,\mathrm{m}$	$2l_2 = 0.1\,\mathrm{m}$	$2l_3 = 0.15\,\mathrm{m}$
$2L_1 = 0.125\,\mathrm{m}$	$H = 2054\,\mathrm{N}$	$H = 1312\,\mathrm{N}$	-
$2L_1 = 0.18\,\mathrm{m}$	$H = 2007.5\,\mathrm{N}$	$H = 1394\,\mathrm{N}$	$H = 845\,\mathrm{N}$

Table 2. Theoretical MOR for cylindrical beams.

	$2l_1 = 0.06\,\mathrm{m}$		$2l_2 = 0.1\,\mathrm{m}$		$2l_3 = 0.15\,\mathrm{m}$	
	$H\,(\mathrm{N})$	$\sigma_{ft}\,(\mathrm{N/m^2})$	$H\,(\mathrm{N})$	$\sigma_{ft}\,(\mathrm{N/m^2})$	$H\,(\mathrm{N})$	$\sigma_{ft}\,(\mathrm{N/m^2})$
$2L_1 = 0.125\,\mathrm{m}$	2054	5.38×10^7	1312	5.73×10^7	-	-
$2L_2 = 0.18\,\mathrm{m}$	2007.5	5.26×10^7	1394	6.09×10^7	845	5.53×10^7

Table 3. 3d numerical MOR for cylindrical beams

	$2l_1 = 0.06\,\mathrm{m}$		$2l_2 = 0.1\,\mathrm{m}$		$2l_3 = 0.15\,\mathrm{m}$	
	$H\,(\mathrm{N})$	$\sigma_{fn}\,(\mathrm{N/m^2})$	$H\,(\mathrm{N})$	$\sigma_{fn}\,(\mathrm{N/m^2})$	$H\,(\mathrm{N})$	$\sigma_{fn}\,(\mathrm{N/m^2})$
$2L_1 = 0.125\,\mathrm{m}$	2054	4.76×10^7	1312	5.32×10^7	-	-
$2L_2 = 0.18\,\mathrm{m}$	2007.5	4.66×10^7	1394	5.65×10^7	845	5.25×10^7

Table 4. Theoretical and numerical MOR for a cylindrical beam of length $2L_1 = 0.125\,\text{m}$.

	σ_{ft} (Pa)	σ_{fn} (Pa)	σ^0_{fn} (Pa)	σ^0_{ft} (Pa)
$2l_1 = 0.06\,\text{m}$	5.38×10^7	4.77×10^7	5.31×10^7	5.16×10^7
$2l_1 = 0.1\,\text{m}$	5.73×10^7	5.32×10^7	5.68×10^7	5.59×10^7

Table 5. Theoretical and numerical MOR for a cylindrical beam of length $2L_2 = 0.18\,\mathrm{m}$.

	σ_{ft} (Pa)	σ_{fn} (Pa)	σ^0_{fn} (Pa)	σ^0_{ft} (Pa)
$2l_1 = 0.06\,\mathrm{m}$	5.26×10^7	4.66×10^7	5.15×10^7	5.04×10^7
$2l_1 = 0.1\,\mathrm{m}$	6.09×10^7	5.65×10^7	6.07×10^7	5.94×10^7
$2l_1 = 0.15\,\mathrm{m}$	5.53×10^7	5.25×10^7	5.49×10^7	5.45×10^7

Table 6. Experimental load of failure and theoretical MOR for beams of square section.

	$2l_1 = 0.06\,\mathrm{m}$		$2l_2 = 0.1\,\mathrm{m}$	
	H	σ_{ft}	H	σ_{ft}
$2L_1 = 0.118\,\mathrm{m}$	$240.1\,\mathrm{N}$	$3.52 \times 10^7 \mathrm{N/m^2}$	$156.8\,\mathrm{N}$	$3.83 \times 10^7 \mathrm{N/m^2}$

Table 7. Theoretical and numerical MOR for a beam of square section of length $2L = 0.118\,\text{m}$.

	σ_{ft} (Pa)	σ_{fn} (Pa)	σ^0_{fn} (Pa)	σ^0_{ft} (Pa)
$2l_1 = 0.06\,\text{m}$	3.52×10^7	3.27×10^7	3.45×10^7	3.37×10^7
$2l_1 = 0.1\,\text{m}$	3.83×10^7	3.63×10^7	3.75×10^7	3.74×10^7